Calculated Hanle transmission and absorption spectra of the ^{87}Rb D_1 line with residual magnetic field for arbitrarily polarized light

Heung-Ryoul Noh[1,*] and Han Seb Moon[2,†]
[1]*Department of Physics, Chonnam National University, Gwangju 500-757, Korea*
[2]*Department of Physics, Pusan National University, Busan 609-735, Korea*
(Received 28 March 2010; published 9 September 2010)

This paper reports a theoretical study on the transmission spectra of an arbitrarily polarized laser beam through a rubidium cell with or without a buffer gas in Hanle-type coherent population trapping (CPT). This study examined how laser polarization, transverse magnetic field, and collisions with buffer gas affects the spectrum. The transmission spectrum due to CPT and the absorption spectrum due to the level crossing absorption (LCA) were calculated according to the laser polarization. The results show that the LCA is strongly dependent on the transverse magnetic field and interaction time of the atoms with a laser light via collisions with the buffer gas. In addition, the spectral shape of the calculated Hanle spectrum is closely related to the direction between the (stray) transverse magnetic field and polarization of the laser.

DOI: 10.1103/PhysRevA.82.033407 PACS number(s): 32.80.Xx, 32.10.Fn, 32.80.Qk

I. INTRODUCTION

There has been considerable interest in the use of atomic coherence in various fields of atomic and molecular physics, such as laser cooling [1], light storage [2–4], atomic magnetometer [5–9], atomic clock [10,11], and quantum information [12–14]. The two important phenomena utilizing atomic coherence, coherent population trapping (CPT) [15] and electromagnetically induced transparency (EIT) [16,17], have been studied extensively in a range of fields due to their broad applications in science and technology. In particular, the CPT in the Hanle configuration has been investigated at length since the first observation of the ground-state Hanle effect owing to its simplicity [18].

Dark and bright resonances occur for the $F_g \rightarrow F_e \leqslant F_g$ and $F_g \rightarrow F_e > F_g$ transitions, respectively, where F_g (F_e) is the total angular momentum of the ground (excited) state. The dark and bright resonances are the phenomena of EIT and electromagnetically induced absorption (EIA) [19–21], respectively. There have been many reports on CPT and EIT experiments in the Hanle configuration using alkali-metal atoms, such as ^{87}Rb, ^{85}Rb, K, and Cs in either a pure or buffer-gas-filled cell [22–36]. In the context of the effect of the external parameters on the CPT spectra, such as a stray magnetic field or the polarization of the laser beam, Nasyrov *et al.* [28] reported a CPT experiment in the Hanle configuration for Cs atoms in a pure cell using an elliptically polarized beam and explained the results using a simple theoretical model. Recently, Huss *et al.* examined the effect of polarization on the Hanle-EIT spectra [29]. They observed a bright resonance for the $F_g = 2 \rightarrow F_e = 1$ transition of ^{87}Rb atoms with circularly polarized light. No absorption would be expected, since the atoms are optically pumped to nonabsorbing states by the circularly polarized light. They explained this phenomenon using a transverse magnetic field which redistributes the population of the magnetic sublevels, resulting in absorption. Quite recently, Yu *et al.* observed subnatural level-crossing absorption and transmission signals using a circularly and linearly polarized beam, respectively, for a Rb cell with a buffer gas [37].

Based on the experimental observation achieved in a previous report [37], this paper reports the results of a detailed theoretical study on the transmission and absorption spectra in the Hanle configuration. The paper is organized as follows. Section II describes the theory used to calculate the Hanle-type CPT spectrum. The calculated results are reported in Sec. III. The final section summarizes the results.

II. THEORY

Figure 1 shows the scheme for the calculation. After passing through a quarter-wave plate ($\lambda/4$ plate), a linearly polarized laser beam in the x direction becomes elliptically polarized and propagates in the z direction, where θ is the angle between the x axis and optic axis of the quarter-wave plate. The incident electric field can be expressed as

$$\vec{E} = E_0\left[e^{-i\theta}\sin\left(\theta+\frac{\pi}{4}\right)\hat{\epsilon}_+ + e^{i\theta}\sin\left(\theta-\frac{\pi}{4}\right)\hat{\epsilon}_-\right], \quad (1)$$

where the spherical bases are defined as $\hat{\epsilon}_\pm = \mp 2^{-1/2}(\hat{x} \pm i\hat{y})$. The laser beam passes through a rubidium cell that is immersed in a magnetic field. In addition to the usual scanning longitudinal magnetic field B_0 along the z direction, a transverse magnetic field B_t is introduced, and the total magnetic field can be expressed as

$$\vec{B} = \hat{z}B_0 + \hat{x}B_t\cos\phi + \hat{y}B_t\sin\phi, \quad (2)$$

where ϕ is the angle between the transverse magnetic field and x axis.

In the absence of a transverse magnetic field, the z axis can be chosen as a quantization axis. However, the direction of the total magnetic field was selected as the quantization axis in the presence of a transverse magnetic field. The electric field in the new coordinate is given as

$$\vec{E} = E_0[A_+\hat{\epsilon}'_+ + A_0\hat{\epsilon}'_0 + A_-\hat{\epsilon}'_-], \quad (3)$$

*hrnoh@chonnam.ac.kr
†hsmoon@pusan.ac.kr

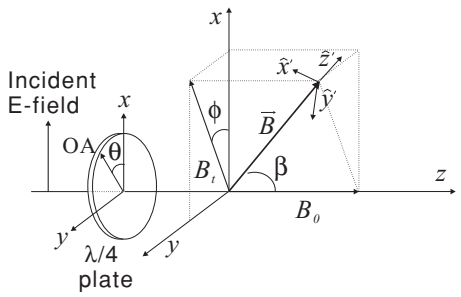

FIG. 1. Schematic diagram to calculate the Hanle spectrum. OA denotes the optical axis of the quarter-wave plate.

where

$$A_{\pm} = \frac{1}{2}e^{i(\phi-\theta)}(1 \pm \cos\beta)\sin\left(\theta + \frac{\pi}{4}\right) + \frac{1}{2}e^{-i(\phi-\theta)}(1 \mp \cos\beta)\sin\left(\theta - \frac{\pi}{4}\right), \quad (4)$$

$$A_0 = -\frac{1}{2}(1+i)\sin\beta[\cos(2\theta-\phi) - i\cos\phi],$$

with $\beta = \tan^{-1}(B_t/B_0)$. In Eq. (3), $\hat{\epsilon}'_{\pm} = \mp 2^{-1/2}(\hat{x}' \pm i\hat{y}')$ and $\hat{\epsilon}'_0 = \hat{z}'$, where the primed Cartesian coordinates are shown in Fig. 1.

In order to calculate the transmission of a laser beam, it is essential to know the susceptibility (χ) for the $F_g = 2 \rightarrow F_e = 1$ transition of the D_1 ^{87}Rb line, which is related to the density-matrix elements as follows [38]:

$$\chi_q = -N_{\rm at}\frac{3\lambda^3}{4\pi^2}\frac{\Gamma}{\Omega_1}\frac{1}{A_q}\sum_{F_e=1}^{2}\sum_{m=-2}^{2} C_{2,m}^{F_e,m+q}\sigma_{2,m}^{F_e,m+q}, \quad (5)$$

where $q = \pm 1$ and 0, $N_{\rm at}$ is the atomic density [39], λ is the resonant wavelength of the D_1 line of ^{87}Rb atoms, Ω_1 is the Rabi frequency of the laser beam, Γ is the decay rate of the excited state, and $\sigma_{F_g,\mu}^{F_e,\nu} = \langle F_e,\nu|\sigma|F_g,\mu\rangle$ is the slowly varying density-matrix element. It should be noted that the off-resonant transition ($F_g = 2 \rightarrow F_e = 2$) was taken into account in Eq. (5), although the laser light was locked at the resonant transition of $F_g = 2 \rightarrow F_e = 1$. This is because in the case of a buffer-gas-filled cell, the decay rate of the excited state due to collision with the buffer-gas atoms is comparable to the excited-state frequency spacing ($\Delta_e = 2\pi \times 814.5$ MHz). Hence we took into account the off-resonant transition ($F_g = 2 \rightarrow F_e = 2$) in the case of the buffer-gas-filled cell, whereas it was neglected in the case of a pure cell. The transitions from the lower ground state ($F_g = 1$) were ignored due to large hyperfine spacing of the ground state (6.8 GHz). In Eq. (5), the normalized transition strength $C_{F_g,m_g}^{F_e,m_e}$ is given by [40]

$$C_{F_g,m_g}^{F_e,m_e} = (-1)^{2F_e+I+J_g+J_e+L_g+S+m_{F_g}+1} \times \sqrt{(2L_e+1)(2J_e+1)(2J_g+1)(2F_e+1)(2F_g+1)} \times \begin{Bmatrix} L_g & L_e & 1 \\ J_e & J_g & S \end{Bmatrix} \begin{Bmatrix} J_g & J_e & 1 \\ F_e & F_g & I \end{Bmatrix} \begin{pmatrix} F_e & 1 & F_g \\ m_e & m_g - m_e & -m_g \end{pmatrix},$$

where L, S, and I represent the orbital, electron spin, and nuclear spin angular momenta, respectively. $(\cdots)$ and $\{\cdots\}$ denote the $3j$ and $6j$ symbols, respectively.

The transmission ($T_0 = I/I_0$) is then given by

$$T_0 \simeq \exp[-kl\,\mathrm{Im}(c_+\chi_+ + c_0\chi_0 + c_-\chi_-)], \quad (6)$$

where I is the intensity after traversing the cell with a length of l, $k = 2\pi/\lambda$, and

$$c_{\pm} = \frac{1}{2}\left(1 \pm \cos\beta\sin 2\theta - \frac{\sin^2\beta}{2}[1 + \cos 2\theta\cos 2(\theta-\phi)]\right), \quad c_0 = \frac{1}{2}\sin^2\beta[1 + \cos 2\theta\cos 2(\theta-\phi)]. \quad (7)$$

The density-matrix elements in Eq. (6) can be calculated from the following density-matrix equation for the $F_g = 2 \rightarrow F_e = 1,2$ transition of the D_1 line of ^{87}Rb atoms:

$$\dot{\rho} = -\frac{i}{\hbar}[H_0 + V, \rho] + \dot{\rho}_{\rm sp}, \quad (8)$$

where ρ is the density operator. The atomic (H_0) and the interaction (V) Hamiltonians are, respectively, given by [41]

$$H_0 = \sum_{m=-2}^{2}\left(\hbar\omega_0 + \hbar\Delta_e + g_{e_2}\mu_B Bm\right)|e_{2,m}\rangle\langle e_{2,m}| + \sum_{m=-1}^{1}\left(\hbar\omega_0 + g_{e_1}\mu_B Bm\right)|e_{1,m}\rangle\langle e_{1,m}| + \sum_{m=-1}^{1} g_g\mu_B Bm|g_m\rangle\langle g_m|, \quad (9)$$

$$V = \frac{1}{2}\hbar\Omega_1\sum_{q=-1}^{1}\sum_{F_e=1}^{2}\sum_{m=-2}^{2} A_q C_{2,m}^{F_e,m+q}|e_{F_e,m+q}\rangle\langle g_m|e^{-i\omega t} + \mathrm{H.c.}, \quad (10)$$

where ω_0 is the resonant frequency and ω is the laser frequency felt by an atom moving with velocity v; $g_{e_2}(=1/6)$, $g_{e_1}(=-1/6)$, and $g_g(=1/2)$ are the Landé g factors of the excited and ground states [42]; and μ_B is the Bohr magneton. In Eq. (8), $\dot{\rho}_{\rm sp}$ denotes the terms associated with spontaneous emission, whose matrix elements are given by [43]

$$\langle e_{F_e,m}|\dot{\rho}_{\rm sp}|e_{F'_e,m'}\rangle = -\Gamma'\langle e_{F_e,m}|\rho|e_{F'_e,m'}\rangle, \quad \langle e_{F_e,m}|\dot{\rho}_{\rm sp}|g_{m'}\rangle = -(\Gamma'/2)\langle e_{F_e,m}|\rho|g_{m'}\rangle, \quad \langle g_m|\dot{\rho}_{\rm sp}|g_{m'}\rangle = \Gamma'\sum_{F_e=1}^{2}\sum_{q=-1}^{1} C_{2,m}^{F_e,m+q}C_{2,m'}^{F_e,m'+q}\langle g_m|\rho|g_{m'}\rangle, \quad (11)$$

where $\Gamma' = \Gamma + \gamma_{\rm coll}$ with $\gamma_{\rm coll}$ being the decay rate of a rubidium atom due to collisions with the buffer gas, and $(\dot{\rho}_{\rm sp})_{ij} = (\dot{\rho}_{\rm sp})_{ji}$ for $i \neq j$. The dephasing decay rate is $\gamma_{\rm coll} = 2\pi \times 500$ MHz [44] when the Ne with 50 Torr of pressure was used as the buffer gas.

The fast time dependence of the density-matrix elements (ρ_{ij}) can be eliminated by transforming into a slowly varying density operator (σ) using the relation $\rho_{ij} = \sigma_{ij}e^{ic_{ij}t}$, where $c_{ij} = -(+)\omega$ for $i \in e_m(g_m)$ and $j \in g_m(e_m)$, and $c_{ij} = 0$ for other i,j values. Equation (8) then becomes

$$\dot{\sigma}_{ij} = e^{-ic_{ij}t}(\dot{\rho})_{ij} - ic_{ij}\sigma_{ij}, \quad (12)$$

where $(\dot{\rho})_{ij}$ are the matrix elements of the operator $\dot{\rho}$ in Eq. (8). It should be noted that the right-hand side of Eq. (12) has no explicit time dependence. Accordingly, there is a set of linear differential equations in Eq. (12). Since an atom is moving with velocity v, Eq. (12) becomes velocity dependent via $\omega \to \omega - kv$. Therefore $\omega = \delta + \omega_0 - kv$ is used, where $\delta = \omega - \omega_0$ is the detuning of the laser frequency.

Finally the transmission in Eq. (6), which is velocity dependent, was averaged over the Maxwell-Boltzmann velocity distribution. In addition, since this study is dealing with time-dependent equations, it is important to average the transmission over the various transit times crossing the laser beam. As described in Ref. [45], the average was obtained simply by integrating the transmission with respect to the transit time. Taking these two averages into account, we have

$$T = \frac{1}{t_{\rm av}} \int_0^{t_{\rm av}} dt \int_{-\infty}^{\infty} dv \frac{1}{\sqrt{\pi} u} e^{-(v/u)^2} T_0(v,t), \qquad (13)$$

where $u = (2k_B T_{\rm cell}/M)^{1/2}$ is the most probable velocity, with $T_{\rm cell}$ being the temperature of the vapor cell and M being the mass of a ^{87}Rb atom. If a pure cell is used, the transit time is given by $t_{\rm av} = (\sqrt{\pi}/2)d/u$, where d is the diameter of the laser beam [46]. In contrast, if a buffer-gas-filled cell is used, the transit time increases by collisions with the buffer gas. This study used $t_{\rm av} = 2.46$ ms, which was calculated using the diffusion coefficient $D = 3.57$ cm^2/s at the pressure of 50 Torr Ne buffer gas [47] and Eq. (1) of Ref. [48].

III. CALCULATED RESULTS AND DISCUSSION

Figure 2 shows the results for the effect of the existence of the off-resonant transition. In Fig. 2, we considered the cell filled with Ne atoms to a pressure of 50 Torr. The temperature of the cell was 70 °C and the laser intensity was 1.3 W/m^2. The magnitude of the transverse magnetic field was assumed to be zero. The angles were $\theta = 27^\circ$ and $\phi = 0^\circ$. In Fig. 2, curve (A) [(D)] denotes the transmission spectrum calculated at the condition of including [excluding] off-resonant transition. Curves (B), (C), and (E) are the results when the excited-state hyperfine spacing was intentionally changed to $2\Delta_e$, $4\Delta_e$, and $-\Delta_e$, respectively. The frequency $-\Delta_e$ implies that the $F_g = 2 \to F_e = 2$ transition line is set to be located artificially below the $F_g = 2 \to F_e = 1$ line. Thus the laser frequency detunings with respect to the transition $F_g = 2 \to F_e = 2$ for spectra (A) and (E) are $-\Delta_e$ and $+\Delta_e$, respectively.

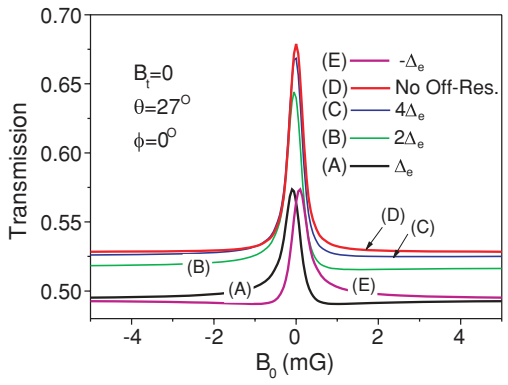

FIG. 2. (Color online) Transmission spectra where the state $|F_e = 2\rangle$ is detuned from the state $|F_e = 1\rangle$ by (A) Δ_e, (B) $2\Delta_e$, (C) $4\Delta_e$, and (E) $-\Delta_e$. Curve (D) denotes the spectrum without the off-resonant transition.

In Fig. 2, when the off-resonant transition is ignored [(D)], the transmission spectrum shows a symmetric line shape. In contrast, when the off-resonant transition is taken into account [(A)], the spectrum becomes asymmetric and is slightly modified due to the effect of the off-resonant transition. Thus in order to accurately calculate the transmission spectrum, it is required to include the off-resonant transition in the excited state. If the frequency spacing of the excited state is increased by a factor of 4 [(C)], the spectrum approaches curve (D) approximately. Taking into account the fact that the ground-state frequency spacing is approximately $8.4\Delta_e$, we may conclude that it is not necessary to include the off-resonant transition from the lower ground state. In what follows, we consider the off-resonant transition in the excited state and neglect the transitions from the ground state $|F_g = 1\rangle$. When we see curves (A) and (E), which correspond to results for the real and artificial $|F_e = 2\rangle$ hyperfine states with the frequency shift of Δ_e and $-\Delta_e$ from the state $|F_e = 1\rangle$, respectively, we can find that two spectra are symmetrical with respect to B_0. Taking into consideration the fact that the EIT and Hanle signals exhibit asymmetric line shapes with the nonresonant laser light and the spectrum is reversed when the laser frequency detuning becomes opposite, we can conclude that the asymmetric line shape is attributed to the off-resonant contribution from the transition $F_g = 2 \to F_e = 2$.

Figure 3 presents the calculation results for various laser polarizations. Figures 3(a) and 3(b) [3(c) and 3(d)] show the transmission spectra for a pure cell and buffer-gas-filled cell, respectively, where the transverse magnetic field is $B_t = 0$ ($B_t \neq 0$). The transverse magnetic fields in Figs. 3(c) and 3(d) were 10 and 1 mG, respectively. In each figure, angle θ between the optic axis and x axis was varied from zero to 45°, while ϕ was fixed at zero. When $\theta = 0$ (45°), the polarization was linear (circular). In Fig. 2, the laser intensity was 1.3 W/m^2 and the diameter was 4.5 mm. The temperature of the pure cell and the buffer-gas-filled cell was 20°C and 70°C, respectively. It was assumed that the buffer-gas cell was filled with Ne atoms to a pressure of 50 Torr. It should be noted that the absolute value of the transmission was adjusted for the signal at $\theta = 0$. For clear comparison, the signals at other angles are shifted upward slightly.

In Figs. 3(a) and 3(b), in the absence of a transverse magnetic field, the amplitude of the resonance signal decreases monotonically with increasing θ from 0° to 45°. In the case of circular polarization, no transmission signal due to the dark resonance signal was observed. When a transverse magnetic field was applied, the signals for the pure cell [Fig. 3(c)] showed no significant variation from the case without the B_t field, whereas a striking variation of the signals was observed in the buffer-gas-filled cell [Fig. 3(d)]. In particular, the signal for the circular polarization shows level crossing absorption (LCA). This phenomenon can be explained by the fact that the population in the magnetic sublevel of the ground state was redistributed due to the transverse magnetic field, which resulted in an increase in absorption.

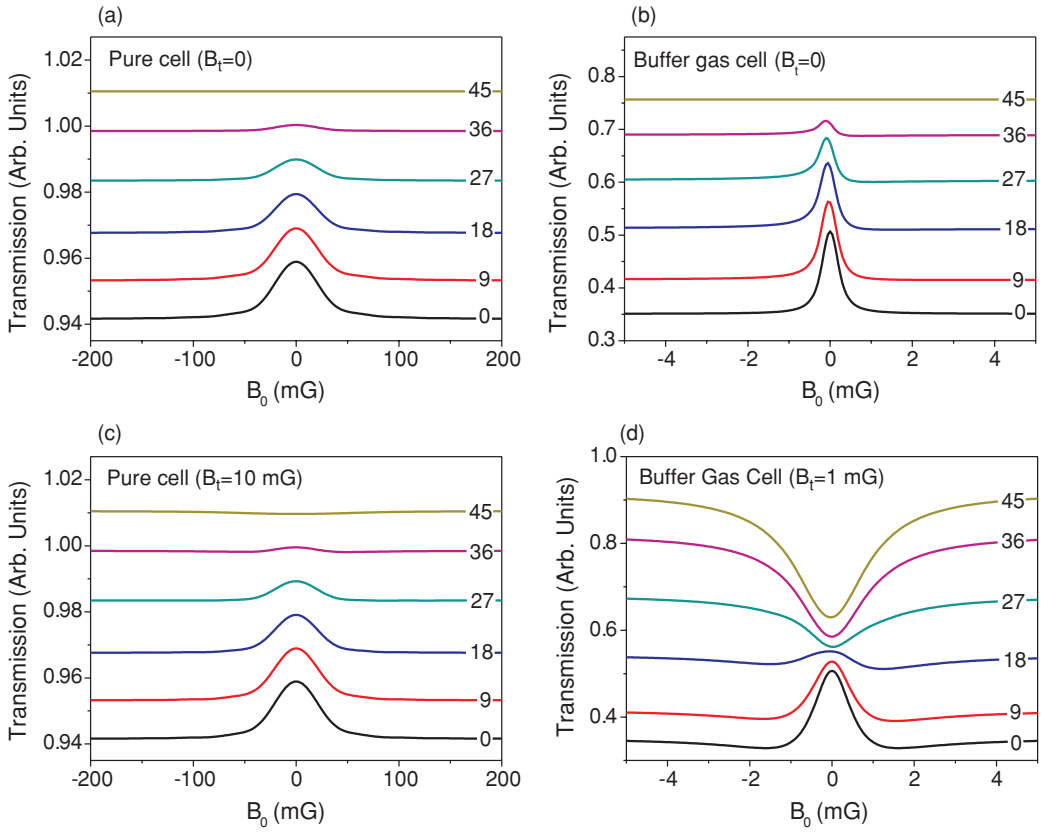

FIG. 3. (Color online) Transmission spectra for the pure (a)[(c)] and buffer-gas-filled cell (b)[(d)] with $B_t = 0$ [$B_t \neq 0$].

The linewidth is reduced if a buffer-gas-filled cell is used because of an increase in the interaction time of the atoms with laser light. A comparison of the results in Figs. 3(c) and 3(d) shows that sufficient interaction time of the atoms with laser light and a transverse magnetic field are needed to observe the LCA signal for circular polarization. A very weak absorption signal was found in the result of $\theta = 45°$, as shown in Fig. 3(c). A detailed study of this phenomenon is described later. In the case of elliptic polarization, the signal showed an asymmetric line shape because of the contribution of the sum of various Lorentzian and dispersive functions.

The effect of the transverse magnetic field in the case of the buffer-gas-filled cell was examined. Figures 4(a), 4(c), and 4(e) [4(b), 4(d), and 4(f)] show the transmission signals as a function of the longitudinal (B_0) and transverse (B_t) magnetic fields, and $\phi = 0$ [$\phi = 90°$]. The polarization is linear ($\theta = 0$) in Figs. 4(a) and 4(b), elliptic ($\theta = 27°$) in Figs. 4(c) and 4(d), and circular ($\theta = 45°$) in Figs. 4(e) and 4(f).

In Fig. 4(a), the transverse magnetic field is directed along the direction of the electric field. The width of the dark resonance signal increases with increasing B_t, whereas the overall line shape does not change significantly. Assuming that the direction of the incident electric field is the quantization axis, in the absence of a magnetic field, the ground sublevels $|g_{\pm 2}\rangle$ are populated due to optical pumping by the π polarized laser beam. Therefore, in this case, a decrease in absorption, i.e., increase in transmission may be observed. While the transverse magnetic field remains zero, as the B_0 field increases, the population of each magnetic sublevel of the ground state begins to be redistributed due to precession of the magnetic moment. Hence, a decrease in the transmission, and accordingly the dark resonance CPT signal can be observed. Since the B_0 required to achieve a redistribution of the population is inversely proportional to the interaction time of the atoms with laser light, a narrow resonance signal can be observed when the interaction time increases using the buffer-gas-filled cell. When a transverse magnetic field is added, the energy level of each ground-state magnetic sublevel changes, and the probability of a population redistribution decreases. Therefore, a larger B_0 field is needed to observe a sufficient absorption signal, which suggests an increase in linewidth for the dark resonance CPT signal.

In contrast, dark resonance can be observed for both B_0 and B_t when the direction of the transverse magnetic field is not collinear with the electric field direction [Fig. 4(b)]. This is because both B_0 and B_t possess a magnetic field component perpendicular to the electric field direction. The high transmission at $B_0 = 0$ and $B_t = 0$ can be reduced when either B_0 or B_t becomes nonzero. The signal at $\phi \neq 0$ was confirmed to be similar to that in Fig. 4(b).

Complicated line shapes can be observed in the case of elliptic polarization [Figs. 4(c) and 4(d)]. The signal varies considerably as B_t varies. As will be discussed later, the transmission signal for these conditions consists of neither a pure dispersive nor a Lorentzian curve, but of complicated combinations of two functions. The detailed studies of the spectra with the elliptically polarized light will be given later.

In the case of circular polarization [Figs. 4(e) and 4(f)], a LCA signal was observed for B_0. The dependence of the signals on the angle ϕ could not be observed because σ^+

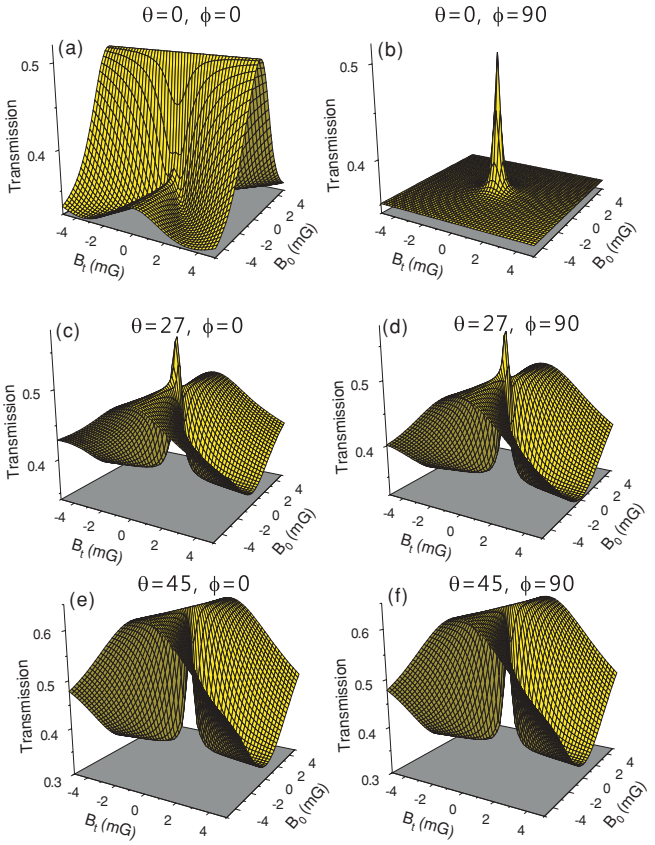

FIG. 4. (Color online) Transmission spectra as functions of the B_0 and B_t fields. $\phi = 0$ [$\phi = 90°$] and $\theta = 0$, $\theta = 27°$, and $\theta = 45°$ for (a) [(b)], (c) [(d)], and (e) [(f)], respectively.

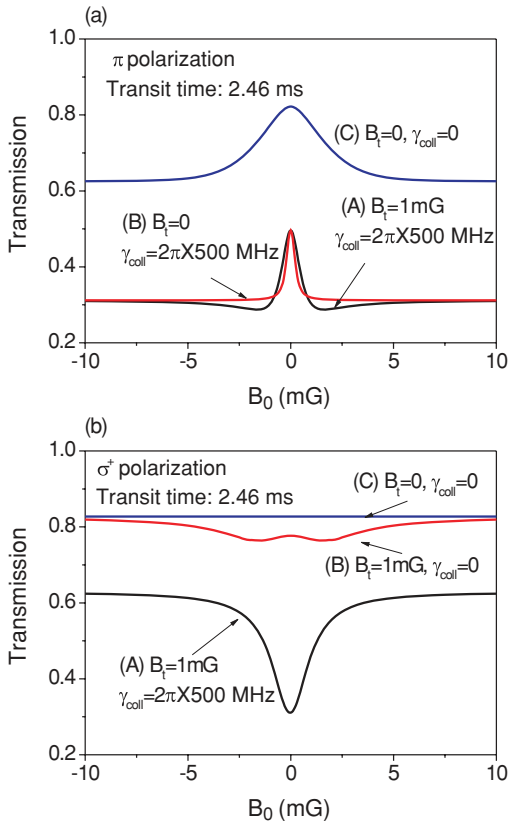

FIG. 5. (Color online) Hanle transmission signals when the polarization is π (a) and σ^+ (b).

polarization was considered. In Figs. 4(e) and 4(f), the LCA signal for B_0 becomes wider with increasing B_t. The range of B_0 showing a LCA signal is approximately proportional to B_t. In the case of σ^+ polarization, the z direction, i.e., the propagating direction of the laser beam, can be chosen as the quantization axis. In the absence of a transverse magnetic field, the atoms are optically pumped to the nonabsorbing ground-state sublevels, $|g_{+1}\rangle$ and $|g_{+2}\rangle$. As a result, no absorption signal is observed regardless of the applied B_0 field. When a transverse magnetic field is applied, the populations of the ground-state sublevels begin to be redistributed provided the magnitude of B_0 is smaller than a threshold value, which results in an absorption signal. For a given B_0, if a larger B_t is applied, a population redistribution would be expedited. Therefore the threshold value of B_0 will be increased, and accordingly, the linewidth of the LCA signal will increase.

In Figs. 4(e) and 4(f), the dark resonance signals for B_t could be observed. This can be explained by the following argument. When the direction of B_t is chosen as a quantization axis, the electric field has a component perpendicular to B_t, which leads to dark resonance signals. A careful comparison of Figs. 4(a) and 4(e) [or 4(f)] enables us to find an opposite role of the B_0 and B_t fields; i.e., the dark resonance and LCA signals for B_0 and B_t in Fig. 4(a), respectively, and vice versa in Fig. 4(e) [or 4(f)]. The reason why the region for the dark resonance signal in Fig. 4(e) [or 4(f)] is narrower than that in Fig. 4(a) is because the component of the electric field perpendicular to B_t in Fig. 4(e) [or 4(f)] is smaller than that perpendicular to B_0 in Fig. 4(a).

The effect of the parameters other than the transit time, which was presented in Fig. 3, on the CPT and LCA signals was examined. Figures 5(a) and 5(b) show the results when the polarization is π and σ^+, respectively. Since the existence of a buffer gas affects both the increase in interaction time and the dephasing of the excited state, it is impossible to separate these two effects in practice. However, these two effects could be examined separately using a calculation. In Fig. 5, while the increase in interaction time due to collisions with the buffer gas was considered, this study examined the dependence of the signal on the transverse magnetic field and the dephasing of the excited state.

In Fig. 5(a), when the polarization is π, the black curve (A) denotes the signal where $B_t = 1$ mG and the dephasing of the excited state is considered. In Fig. 5, considering the dephasing implies the usual case for a buffer-gas-filled cell. The result denoted by the red curve (B), where $B_t = 0$ and the dephasing is considered, shows a slight variation from the black curve (A). Therefore, the effect of the transverse magnetic field was very weak in the case of linear polarization. The red curve (C) presents the result where $B_t = 1$ mG and the dephasing was not considered. In this case, signal broadening was observed. Therefore, in Fig. 5(a), when the polarization is π, as well as an increase in transit time due to collision of the atoms with the buffer gas, the increase in decay rate resulting from collisions with the buffer gas also affects the linewidth of the dark resonance Hanle signal. This is because

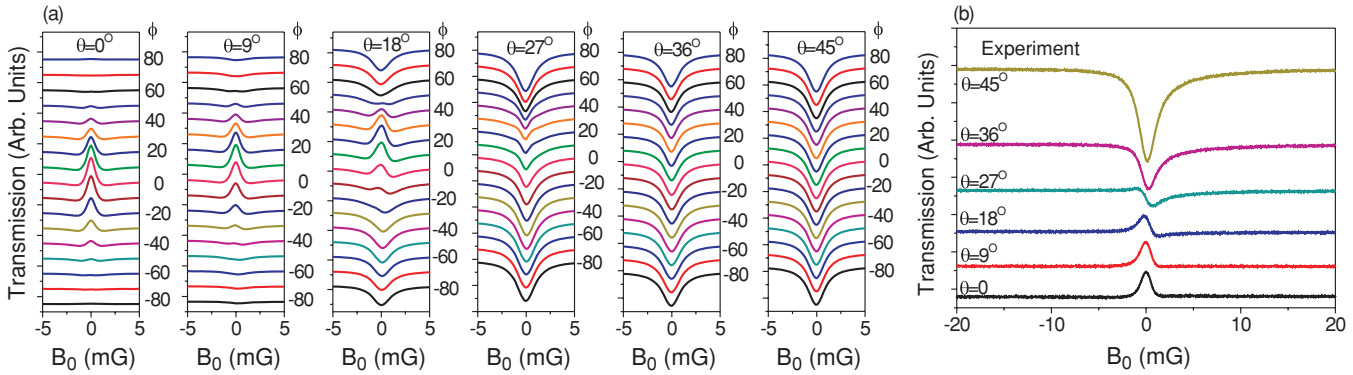

FIG. 6. (Color online) (a) Calculated transmission signals depending on θ and ϕ. (b) Experimental results at $\theta = 0$, 9°, 18°, 27°, 36°, and 45°.

transfer of the atomic population into the states $|g_{\pm 2}\rangle$, which are nonabsorbing states, is expedited due to the increase in the decoherence rate of the excited state. A comparison of (A) and (B) in Fig. 5(a) showed that the effect of the transverse magnetic field is quite weak. This study also checked the condition when only the dephasing of the excited state was considered, whereas the transit time was limited to the value for the case of a pure cell. It was observed that the linewidth of the CPT signal was similar to that observed in the case of the pure cell. Therefore, in the case of linear polarization, the most important factor for linewidth narrowing is an increase in transit time followed by dephasing of the excited state. In reality, these two occur simultaneously.

Figure 5(b) shows the results when the polarization is circular. In Fig. 5(b), the black curve (A) denotes the result obtained under the condition when $B_t = 1$ mG and the dephasing is considered. A narrow LCA signal could be observed. When the effect of dephasing was removed from curve A, i.e., in the red curve (B), the absorption signal was suppressed. No absorption signal was observed when the effect of the transverse magnetic field was further removed [blue curve (C)]. Therefore, when the polarization was circular [Fig. 5(b)], the LCA signal resulted mainly from the transverse magnetic field. In the absence of a transverse magnetic field (C), there was no absorption signal irrespective of whether the dephasing existed or not.

Once B_t was applied (B), the absorption signal arose. The LCA signal increased further when the effect of a buffer gas on the increase in decay rate of the excited state was considered. This is because the decoherence between the magnetic sublevels in the excited state transfers to the ground state and results in increased mixing of the populations in the ground state. From Figs. 3(d) and 5(b), the B_t value needed to observe the absorption signal decreases with increasing collision decay rate due to buffer gas. Therefore, in the case of the circular polarization, the transverse magnetic field is the most important factor for the LCA signal followed by the increase in transit time. When these two conditions are satisfied, the addition of dephasing further increases the LCA signal.

The effect of ϕ, which is the angle between the x axis and the transverse magnetic field direction, was next considered. Figure 6(a) shows the transmission spectra where $\theta = 0°$, 9°, 18°, 27°, 36°, and 45° from left to right. It was assumed that $B_t = 1$ mG and the transit time was 2.46 ms. In each column the spectra for ϕ such that $-80° \leqslant \phi \leqslant 80°$ with a step of 10° are presented. When $\theta = 0°$ and 9°, i.e., the polarization is approximately linear, the magnitude of the dark resonance signal varies significantly for different ϕ values, even though the overall characteristics of dark resonance are maintained. The amplitude of the dark resonance was largest when $\phi = 0°$, i.e., the electric vector of the incident (approximately) linearly polarized laser beam was directed approximately along the direction of the transverse magnetic field. This effect was already observed in Figs. 4(a) and 4(b) and explained previously.

When the circular polarization dominated, i.e., $\theta = 36°$ and 45°, the bright resonance signal did not change significantly with ϕ. This was also observed in Figs. 4(e) and 4(f). The insensitivity of the signal to ϕ could be used to determine the magnitude of the transverse magnetic field. A comparison with the experimental results presented in Ref. [37] showed that the magnitude of the transverse magnetic field was approximately 1 mG.

Consider the case of elliptic polarizations ($\theta = 18°$ and $\theta = 27°$). In these cases, in particular when $\theta = 18°$, the spectrum varies strikingly according to the value of ϕ. Therefore, information obtained at the condition of the elliptic polarization may be used to determine the angle between the x axis and the direction of the transverse magnetic field. Figure 6(b) shows the experimental results presented in a previous report [37]. A rough comparison of Figs. 6(a) and 6(b) shows that the value ϕ of the experimental result resides approximately in the range of $\phi = 0° \sim 30°$. The line shape of the spectrum depends on many parameters such as spatially nonuniform magnetic field or imperfect polarization of laser light. Thus to more precisely determine the angle ϕ, it is required to elaborate the experimental conditions such as, especially, reduction of the magnetic field inhomogeneity. The experiment in an improved setup is currently under way.

IV. CONCLUSIONS

This paper reports the results of a theoretical study of LCA and CPT in the Hanle configuration for an arbitrarily polarized laser beam. The linewidth narrowing of the CPT signal for

a linearly polarized laser beam was studied. Two important factors were determined to have a significant effect: an increase in atomic transit time in the vapor cell due to collisions with the buffer gas and dephasing of the excited-state population. The observed LCA for the circularly polarized laser beam was attributed to the effect of the transverse magnetic field. The absorption signal was increased further by the increase in transit time in the buffer-gas-filled cell. We also studied the effect of the off-resonant transition. We found that, in the case of a buffer-gas-filled cell, the spectrum becomes asymmetric and its magnitude is changed compared to the spectrum obtained without the off-resonant transition.

The change in the transmission spectrum was also investigated according to the longitudinal (scanning) and transverse magnetic field for various polarizations of the laser beam and the angle (ϕ) between the x axis and transverse magnetic field. Interestingly, the longitudinal and transverse magnetic fields were found to play an opposite role in the cases of linear and circular polarizations. The insensitivity of the LCA signal in the case of circular polarization can be used in the accurate determination of the magnitude of the stray transverse magnetic field. The striking variation of the signals for the elliptic polarized light may be used for determination of the direction of a stray transverse magnetic field.

ACKNOWLEDGMENTS

This work was supported by the Korea Research Foundation Grant funded by the Korean Government (KRF-2008-313-C00355 and KRF-2008-314-C00075).

[1] H. J. Metcalf and P. van der Straten, *Laser Cooling and Trapping* (Springer, New York, 1999).
[2] C. Liu, Z. Dutton, C. H. Behroozi, and L. V. Hau, Nature **409**, 490 (2001).
[3] M. Bajcsy, A. S. Zibrov, and M. D. Lukin, Nature **426**, 638 (2003).
[4] M. D. Lukin, Rev. Mod. Phys. **75**, 457 (2003).
[5] D. Budker and M. V. Romalis, Nature Phys. **3**, 227 (2007).
[6] I. K. Kominis, T. W. Kornack, J. C. Allred, and M. V. Romalis, Nature **422**, 596 (2003).
[7] R. Wynands and A. Nagel, Appl. Phys. B **68**, 1 (1999).
[8] C. Andreeva, G. Bevilacqua, V. Biancalana, S. Cartaleva, Y. Dancheva, T. Karaulanov, C. Marinelli, E. Mariotti, and L. Moi, Appl. Phys. B **76**, 667 (2003).
[9] P. D. D. Schwindt, S. Knappe, V. Shah, L. Hollberg, J. Kitching, L.-A. Liew, and J. Moreland, Appl. Phys. Lett. **85**, 6409 (2004).
[10] S. Knappe, V. Shah, P. D. D. Schwindt, L. Hollberg, J. Kitching, L.-A. Liew, and J. Moreland, Appl. Phys. Lett. **85**, 1460 (2004).
[11] H. S. Moon, S. E. Park, Y. H. Park, L. Lee, and J. B. Kim, J. Opt. Soc. Am. B **23**, 2393 (2006).
[12] A. Kuzmich, W. P. Bowen, A. D. Boozer, A. Boca, C. W. Chou, L.-M. Duan, and H. J. Kimble, Nature **423**, 731 (2003).
[13] C. Ottaviani, D. Vitali, M. Artoni, F. Cataliotti, and P. Tombesi, Phys. Rev. Lett. **90**, 197902 (2003).
[14] K. Hammerer, A. S. Sørensen, and E. S. Polzik, Rev. Mod. Phys. **82**, 1041 (2010).
[15] E. Arimondo, Prog. Opt. **35**, 257 (1996).
[16] S. E. Harris, Phys. Today **50**, 36 (1997).
[17] M. Fleischhauer, A. Imamoglu, and J. P. Marangos, Rev. Mod. Phys. **77**, 633 (2005).
[18] J. C. Lehmann and C. Cohen-Tannoudji, C.R. Acad. Sci. **258**, 4463 (1964).
[19] A. M. Akulshin, S. Barreiro, and A. Lezama, Phys. Rev. A **57**, 2996 (1998).
[20] A. V. Taichenachev, A. M. Tumaikin, and V. I. Yudin, Phys. Rev. A **61**, 011802(R) (1999).
[21] S. K. Kim, H. S. Moon, K. Kim, and J. B. Kim, Phys. Rev. A **68**, 063813 (2003).
[22] F. Renzoni, W. Maichen, L. Windholz, and E. Arimondo, Phys. Rev. A **55**, 3710 (1997).
[23] Y. Dancheva, G. Alzetta, S. Cartaleva, M. Taslakov, and Ch. Andreeva, Opt. Commun. **178**, 103 (2000).
[24] G. Alzetta, S. Cartaleva, Y. Dancheva, Ch. Andreeva, S. Gozzini, L. Botti, and A. Rossi, J. Opt. B **3**, 181 (2001).
[25] C. Andreeva, S. Cartaleva, Y. Dancheva, V. Biancalana, A. Burchianti, C. Marinelli, E. Mariotti, L. Moi, and K. Nasyrov, Phys. Rev. A **66**, 012502 (2002).
[26] G. Alzetta, S. Gozzini, A. Lucchesini, S. Cartaleva, and T. Karaulanov, C. Marinelli, and L. Moi, Phys. Rev. A **69**, 063815 (2004).
[27] S. Gateva, E. Alipieva, and E. Taskova, Phys. Rev. A **72**, 025805 (2005).
[28] K. Nasyrov, S. Cartaleva, N. Petrov, V. Biancalana, Y. Dancheva, E. Mariotti, and L. Moi, Phys. Rev. A **74**, 013811 (2006).
[29] A. Huss, R. Lammegger, L. Windholz, E. Alipieva, S. Gateva, L. Petrov, E. Taskova, and G. Todorov, J. Opt. Soc. Am. B **23**, 1729 (2006).
[30] C. Andreeva, A. Atvars, M. Auzinsh, K. Blush, S. Cartaleva, L. Petrov, and D. Slavov, Phys. Rev. A **76**, 063804 (2007).
[31] M. Auzinsh, R. Ferber, F. Gahbauer, A. Jarmola, and L. Kalvans, Phys. Rev. A **78**, 013417 (2008).
[32] M. Auzinsh, R. Ferber, F. Gahbauer, A. Jarmola, and L. Kalvans, Phys. Rev. A **79**, 053404 (2009).
[33] S. Gozzini, S. Cartaleva, A. Lucchesini, C. Marinelli, L. Marmugi, D. Slavov, and T. Karaulanov, Eur. Phys. J. D **53**, 153 (2009).
[34] A. Vilardi, D. Tabarelli, L. Botti, A. Bertoldi, and L. Ricci, J. Phys. B **42**, 055003 (2009).
[35] M. Radonjić, D. Arsenović, Z. Grujić, and B. M. Jelenković, Phys. Rev. A **79**, 023805 (2009).
[36] A. J. Krmpot, S. M. Ćuk, S. N. Nikolić, M. Radonjić, D. G. Slavov, and B. M. Jelenković, Opt. Express **17**, 22491 (2009).
[37] Y. J. Yu, H. J. Lee, I. H. Bae, H. R. Noh, and H. S. Moon, Phys. Rev. A **81**, 023416 (2010).
[38] D. Meschede, *Optics, Light and Lasers* (Wiley-VCH, Weinheim, 2007).
[39] P. Siddons, C. S. Adams, C. Ge, and I. G. Hughes, J. Phys. B **41**, 155004 (2008).
[40] A. R. Edmonds, *Angular Momentum in Quantum Mechanics* (Princeton University Press, Princeton, 1960).
[41] C. Cohen-Tannoudji, J. Dupont-Roc, and G. Grynberg, *Atom-Photon Interactions, Basic Processes and Applications* (Wiley, New York, 1992).
[42] See [http://steck.us/alkalidata]

[43] H. Failache, P. Valente, G. Ban, V. Lorent, and A. Lezama, Phys. Rev. A **67**, 043810 (2003).

[44] E. E. Mikhailov, I. Novikova, Y. V. Rostovtsev, and G. R. Welch, Phys. Rev. A **70**, 033806 (2004).

[45] H. R. Noh and H. S. Moon, Phys. Rev. A **80**, 022509 (2009).

[46] J. Sagle, R. K. Namiotka, and J. Huennekens, J. Phys. B **29**, 2629 (1996).

[47] I. Novikova, Y. Xiao, D. F. Phillips, and R. L. Walsworth, J. Mod. Opt. **52**, 2381 (2005).

[48] I. Novikova, A. B. Matsko, and G. R. Welch, J. Opt. Soc. Am. B **22**, 44 (2005).